Microsc. Microanal. 7, 356–362, 2001
DOI: 10.1007/s10005-001-0003-5

Microscopy AND Microanalysis

Scattering Cross Sections in Electron Microscopy and Analysis

Peter Rez

Department of Physics and Astronomy, and Center for Solid State Science, Arizona State University, Tempe, AZ 85287

Abstract: The scattering cross section is the fundamental measure of the strength of a scattering interaction. All scattering in electron microscopy arises from the Coulomb interaction, and scattering cross sections, whether elastic or inelastic, will therefore all have common features. Simple forms of both elastic and inelastic cross sections are reviewed in the context of high resolution and analytical microscopy. Some recent developments, such as the calculation of Fano resonances in electron energy loss spectra of transition metals and rare earth elements are also discussed.

Key words: scattering cross section, analytical electron microscopy, transition metal elements, rare earth elements, electron energy loss spectrometry, Fano resonance

Introduction

The electron microscope is not only an imaging device but also a scattering chamber with excellent control of many of the variables that define a scattering interaction. In all scattering experiments, some measure is needed of the strength of the scattering interaction. The scattering cross section, which has dimensions of area, is a quantity that can be defined for any scattering interaction, irrespective of the nature of the scatterer, or the particle or radiation being scattered. To define a scattering cross section, refer to the geometry of Figure 1. If I_0 is the incident number of particles (or current), I_S is the number of particles (or current) scattered through an angle θ with an energy loss ΔE, N is the number of scatterers/unit volume, and t is the thickness of the specimen (or length of the scattering region) then

$$I_S\,(\theta, \Delta E) = Nt\sigma(\theta, \Delta E)I_0 \qquad (1)$$

Received November 6, 1999; accepted November 20, 1999.

where $\sigma(\theta,\Delta E)$ is the scattering cross section. The product Nt represents the number of scatterers per unit area as seen by the incident beam. The cross section defined above is a double-differential scattering cross section, sometimes denoted by $d^2\sigma/dEd\Omega$, as it represents the variation of strength of scattering with scattering angle and energy loss. A differential scattering cross section denoted by $d\sigma/d\Omega$ describes the variation with scattering angle when the energy loss is not explicitly recorded. Integrating over a range (or all) scattering angles gives a total scattering cross section.

In electron microscopy, all scattering is due to the Coulomb interaction between the probing electron, coordinate $\mathbf{r}$, and an electron or ion in the specimen, coordinate $\mathbf{r}'$. To calculate the scattering cross section, a scattering rate, W, is first calculated using Fermi's Golden Rule. This is derived from first-order time-dependent perturbation theory (Schiff, 1968) in which the Coulomb interaction is the perturbation

$$H' = \frac{e^2}{4\pi\varepsilon_0|\mathbf{r} - \mathbf{r}'|}\,. \qquad (2)$$

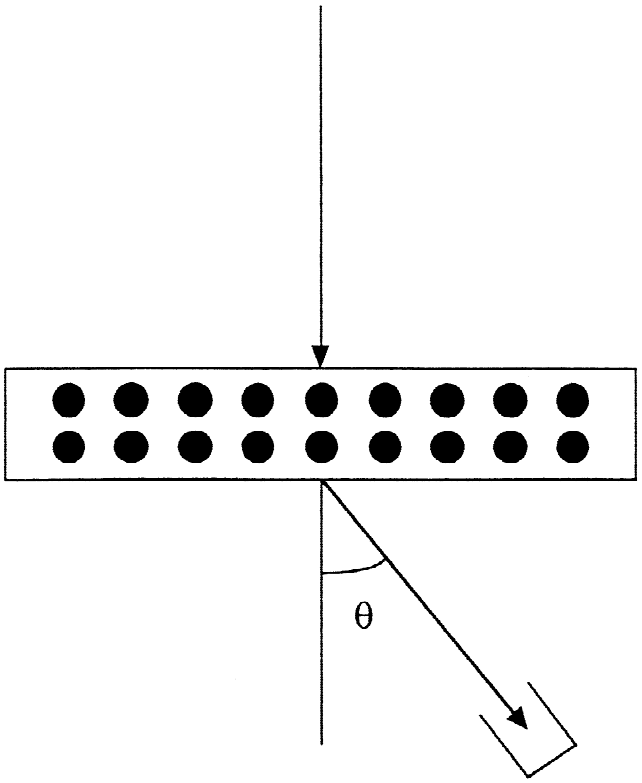

Figure 1. Scattering geometry.

A simple analysis based on equation (1) shows that the scattering cross section is the scattering (or transition) rate divided by the velocity, v, of the incoming particles.

$$\frac{I_s}{I_0} = \frac{n}{A}\frac{W}{v} = Nt\sigma \tag{3}$$

In transmission microscopy, exchange processes between the probing, or fast (sometimes called the swift), electron and the specimen electron are negligible. The total wavefunction can therefore be represented as a product of the fast electron wavefunction $\psi(\mathbf{r}')$ and the electron in the solid $\phi(\mathbf{r})$. As an example, the cross section for a transition from initial state i to final state f is

$$\sigma = \frac{2\pi}{\hbar v}\rho(E) \left|\iint \psi_f(\mathbf{r}')\phi_f(\mathbf{r})\left|\frac{e^2}{4\pi\varepsilon_0|\mathbf{r}-\mathbf{r}'|}\right|\varphi_i(\mathbf{r})\psi_i(\mathbf{r}')d^3r d^3r'\right|^2 \tag{4}$$

where $\rho(E)$ is the density of fast electron final states.

At this point, we make an important simplification and assume that the probing or fast electron states can be represented as plane waves. The term cross section has been used in the electron microscopy and diffraction literature (Allen, 1993) to denote a measure of scattering strength in quite general conditions where there is mixed multiple elastic (dynamical) scattering and inelastic scattering. I believe that the term should only be used for a simple, single-scattering experiment that can be described by equation (1), where the amount of scattering is linear in specimen thickness.

Substituting $\psi_i(\mathbf{r}') = \exp(i\mathbf{k}_i.\mathbf{r}')$ for the fast electron initial state and $\psi_f(\mathbf{r}') = \exp(i\mathbf{k}_f.\mathbf{r}')$ for the final state, then integrating over the fast electron coordinate $\mathbf{r}'$ gives the general expression for the double differential scattering cross section

$$\frac{d^2\sigma}{d\Omega dE} = \frac{4\gamma^2}{a_0^2}\frac{k_f}{k_i}\frac{\left|\int \varphi_f^*(\mathbf{r}')\exp(i\mathbf{q}.\mathbf{r}')\varphi_i(\mathbf{r}')d^3\mathbf{r}'\right|^2}{q^4} \tag{5}$$

where $\mathbf{q} = \mathbf{k}_i - \mathbf{k}_f$ is the momentum transfer in the scattering event and γ is the relativistic factor

$$\gamma = \frac{1}{\sqrt{1-\dfrac{v^2}{c^2}}}.$$

The constant $4/a_0^2$, where a_0 is the Bohr radius, is fundamental to the Coulomb interaction and immediately gives an approximate scale for electron beam interactions in the electron microscope.

Elastic Scattering

When the probing electron loses no energy while passing through the specimen and leaves the specimen unchanged, the interaction is called elastic scattering. The final and initial states of the crystal electrons are the same and so $\varphi_f^*(\mathbf{r}')$ can be replaced by $\varphi_i^*(\mathbf{r}')$. The probing electron not only interacts with the electrons in the specimen but may also scatter from the nuclei. Equations (1) and (4) should be modified by adding a term representing the Coulomb interaction between the fast electron and a nucleus at position $\mathbf{R}$, with atomic number Z. Equation (4) now becomes

$$\sigma = \frac{2\pi}{\hbar v}\rho(E)\left|\int \psi_f^*(\mathbf{r}')\left|\frac{Ze^2}{4\pi\varepsilon_0|\mathbf{R}-\mathbf{r}'|} - \sum_i \int \phi_i(\mathbf{R}+\mathbf{r})\left|\frac{e^2}{4\pi\varepsilon_0|\mathbf{R}+\mathbf{r}-\mathbf{r}'|}\right|\varphi_i(\mathbf{R}+\mathbf{r})d^3\mathbf{r}\right|\psi_i(\mathbf{r}')d^3\mathbf{r}'\right|^2 \tag{6}$$

where interactions with all the electrons associated with the atom, denoted by index *i,* are summed. This expression can be much simplified once it is recognized that the sum over the square of the wave functions for electrons associated with an atom is the atomic charge density.

$$\rho(\mathbf{R}+\mathbf{r}) = \sum_i \varphi_i^*(\mathbf{R}+\mathbf{r})\varphi_i(\mathbf{R}+\mathbf{r}) \tag{7}$$

Assuming the fast or probing electron states can still be represented by plane waves, the differential scattering cross section can be derived by integrating over the fast electron coordinate $\mathbf{r}'$ and can be written as

$$\frac{d\sigma}{d\Omega} = \frac{4\gamma^2}{a_0^2}\frac{\left[Z - \int \rho(\mathbf{r})\exp(i\mathbf{q}.\mathbf{r})d^3\mathbf{r}\right]^2}{q^4} = \frac{4\gamma^2}{a_0^2}\frac{[Z - f_x(q)]^2}{q^4} = |f_{el}(q)|^2. \tag{8}$$

The scattering from the atomic electrons appears as the Fourier transform of the charge density which is the X-ray scattering factor $f_x(q)$. In kinematical treatments of electron diffraction, it is convenient to define an electron scattering factor which is used in exactly the same way as the X-ray scattering factor. The differential cross section is the square of the modulus of the electron scattering factor, which in general can be a complex quantity. The relationship between the X-ray and electron scattering factors (Hirsch et al., 1965), given by equation (8), is known as the Mott formula for the electron scattering factor.

It is instructive to take various limits to understand the behavior of elastic Coulomb scattering. For small scattering wave vectors, q, the X-ray scattering factor tends to the atomic number for neutral atoms

$$f_x(q) = Z - \alpha q^2 \tag{9}$$

where α is a constant which can be related to mean square size of the atom. (For ions, Z should be replaced by the number of electrons, which means that for a single ion, the scattering factor becomes infinite. It should be remembered that for overall charge neutrality there must be equal numbers of positive and negative ions, and the infinite terms all cancel.) Using equation (9), the limit of the differential cross section becomes

$$\frac{d\sigma}{d\Omega} = \frac{4\gamma^2}{a_0^2}\alpha^2 . \tag{10}$$

In recent years, high-angle annular dark-field (HAADF) microscopy has become popular as a technique since it not only gives atomic resolution but also shows a high degree of atomic specificity (Pennycook and Boatner, 1988). Early arguments appealed to the idea that, at high angles or momentum transfers, only the Rutherford scattering from the nucleus was significant and, according to equation (8), the cross section should scale as the square of the atomic number.

$$\frac{d\sigma}{d\Omega} = \frac{4\gamma^2}{a_0^2}\frac{Z^2}{q^4} \tag{11}$$

More sophisticated treatments have shown that the high angle scattering arises from multiphonon or thermal diffuse scattering (Jesson and Pennycook, 1995; Amali and Rez, 1997). A simple derivation assuming independently vibrating atoms gives the following expression

$$\frac{d\sigma}{d\Omega} = \frac{4\gamma^2}{a_0^2}\frac{[Z - f_x(q)]^2}{q^4}[1 - \exp(-2Mq^2)] \tag{12}$$

for the differential cross section, where M is the Debye-Waller factor. The high angle behavior of the Rutherford cross section [equation (11)], the Mott formula [equation (8)], and thermal diffuse scattering [equation (12)] are shown as Figure 2 for scattering of 100 kV electrons from silicon. A logarithmic plot is used to accommodate the dynamic range of almost 10^{12}. As expected, the Rutherford cross section is unrealistic for small angles since it becomes infinite. The thermal diffuse scattering tends to zero much faster than the Mott formula, showing that thermal diffuse scattering is mainly important at high scattering angles. In the high-angle regime, the Mott formula and the thermal diffuse cross sections become very close above 80 mrad, but both are still much less than the Rutherford cross section. Of course, for materials with a lower Debye-Waller factor, the divergence between elastic scattering given by the Mott formula and thermal diffuse scattering might persist to higher scattering angles.

Experimentally, all the intensity recorded by a detector over a range of scattering angles accepted by the detector is measured. This is an integrated cross section and, in Figure 3, the integrated cross sections for scattering between a

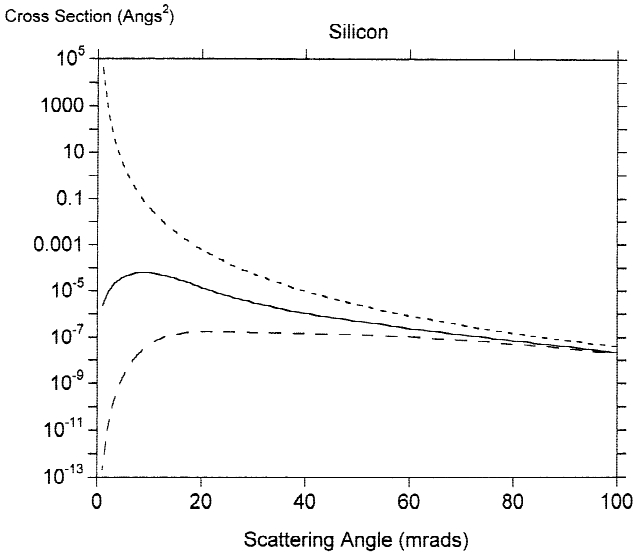

Figure 2. Differential scattering cross section as a function of scattering angle for 100 kV electrons incident on silicon. Short dashed line, Rutherford cross section; solid line, Mott formula; long dashed line, thermal diffuse scattering.

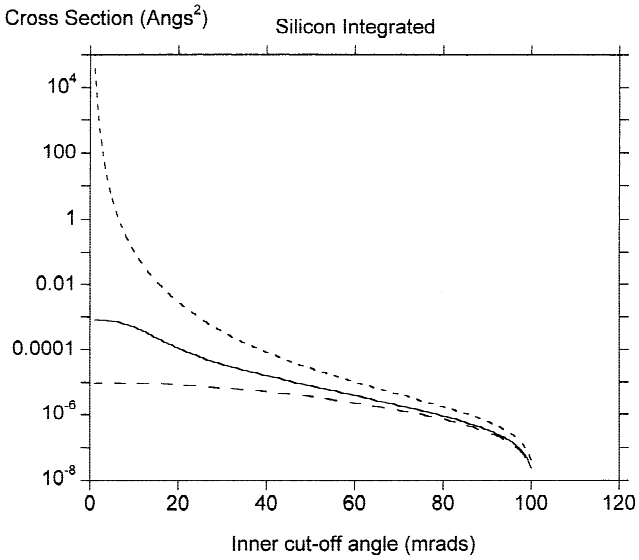

Figure 3. High-angle annular dark-field (HAADF) integrated cross section as a function of inner cut-off angle for 100 kV electrons incident on silicon. The outer cut-off angle is assumed to be 100 mrad. Short dashed line, Rutherford cross section; solid line, Mott formula; long dashed line, thermal diffuse scattering.

given angle (the inner cut-off angle) and 100 mrads (the outer cut off) are plotted for the same cross sections as displayed in Figure 2. The same trends are again apparent, though it is interesting to note that the elastic scattering from the Mott formula is almost saturated for an inner cut off between 5 and 10 mrads. Calculations for scattering of 300 kV electrons show a similar behavior allowing for the different range of scattering angles, since all the cross sections are functions of momentum transfer.

The significant result from Figures 2 and 3 is that scattering from atomic electrons is still important, even at high angles, and that the bare Rutherford cross section should not be used for quantitative analysis.

Inelastic Scattering

The general form for the differential scattering cross section has already been given as equation (5). By analogy with X-ray and optical absorption, this expression is often written in terms of a generalized oscillator strength defined by (see Egerton, 1986):

$$\frac{df(q,E)}{dE} = \frac{2mE}{\hbar^2 q^2}\left|\int \varphi_f^*(\mathbf{r}')\,\exp(i\mathbf{q}.\mathbf{r}')\varphi_i(\mathbf{r}')d^3\mathbf{r}'\right| \quad (13a)$$

$$\frac{d^2\sigma}{d\Omega dE} = \frac{4}{a_0^2 q^2}\frac{k_f}{k_i}\frac{\hbar^2}{2mE}\frac{df(q,E)}{dE}. \quad (13b)$$

The behavior of the generalized oscillator strength has been extensively studied for inner shell excitations using atomic theory. A full knowledge of the generalized oscillator strength makes it possible to calculate the partial cross section for any specified collection angle, accelerating voltage or integration range of energies used in energy loss microanalysis (Leapman et al., 1980). In many cases, especially for collection angles below about 10 mrad for typical microscope operating voltages, it is possible to make the approximation that $\mathbf{q}.\mathbf{r}' < 1$ and the exponential can be expanded to first order. Since the initial and final states are orthogonal, the differential cross section reduces to the dipole form

$$\frac{d^2\sigma}{d\Omega dE} = \frac{4}{a_0^2 q^2}\left|\int \varphi_f^*(\mathbf{r}')\mathbf{r}'\varphi_i(\mathbf{r}')d^3\mathbf{r}'\right|^2. \quad (14)$$

The integral over the angular parts of the wave function leads to the dipole selection rule that the final state angular momentum l' is given by $l' = l + 1$ where l is the initial state

angular momentum. In practice, it is often possible to analyze fine structures under a wide variety of conditions using this simple rule (Rez et al., 1995).

The double-differential cross section for a particular inner shell ionization can be integrated over all scattering angles and all possible energy losses to obtain a total ionization cross section for that particular shell (or subshell) (Scofield, 1978; Rez, 1984). The X-ray production cross section can be obtained by multiplying by the fluorescence yield, which is the probability of the ionization decaying by X-ray emission. All cross sections of relevance to microanalysis can be calculated on the basis of the Coulomb scattering outlined above.

Partial cross sections based on Hartree-Slater cross sections have proven to be quite accurate in many cases (better than 5% for K shells, 10% for L shells and the M_{45} excitations of the rare earths) (Auerhammer et al., 1989). There are cases where the simple model of excitation from an inner shell to a single continuum state is no longer adequate. The 3p (M_{23}) edges in the first row transition elements and the N_{45} (4d) edges in the rare earths are marked by an anomalously high cross section just after threshold, sometimes preceded by a dip in the region before the edge. These edges are dominated by an interference effect called a Fano resonance.

Fano Resonances

A Fano resonance can arise when there is an unfilled bound state (3d for the transition elements and 4f for the rare earths) accessible by a dipole transition from the inner shell that is being excited. Since the mechanics of the process are the same for both the transitional element M_{23} edges and the rare earth N_{45} edges, we shall for simplicity only consider the transition element case. The complete theory was originally published by Fano (1961) and later elaborated by Davis and Feldkamp (1977), and Starace (1974). The final state wave function should be written as a linear combination of the continuum d states and the bound 3d state

$$\varphi_f = a\varphi_{3d} + \int b_{\varepsilon'}\varphi_{\varepsilon' d}\, d\varepsilon'. \tag{15}$$

The problem reduces to determining the coefficients a and b as functions of energy. Formally we now have a two configuration system with a term in the Hamiltonian representing the configuration interaction V_ε.

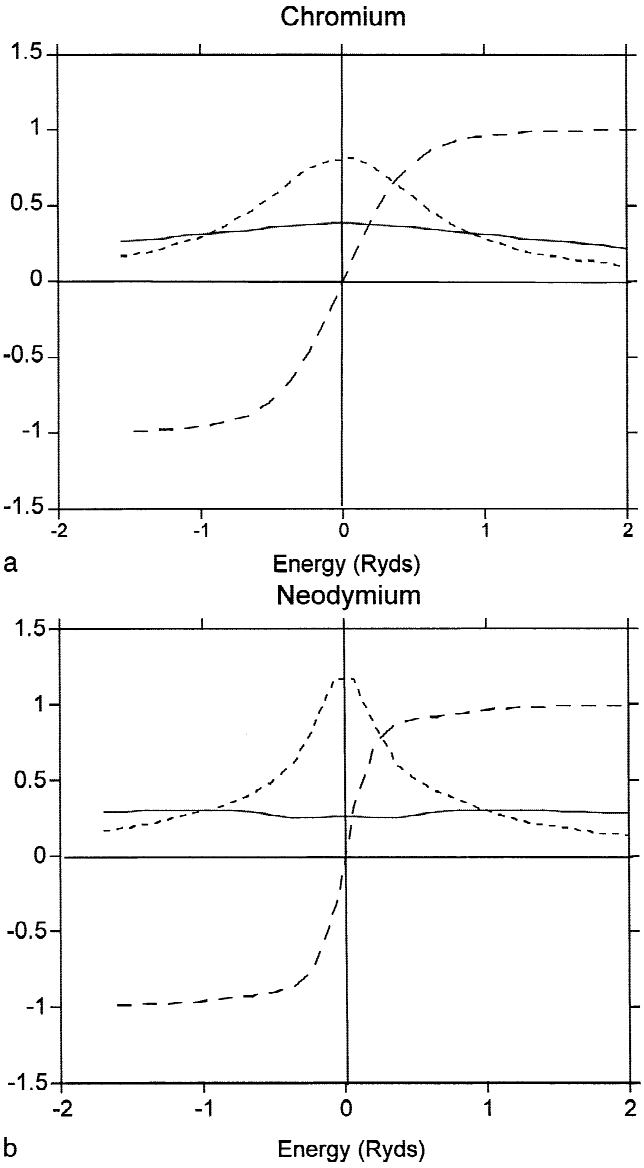

Figure 4. Variation with energy of the square of configuration interaction integral V_ε^2 (solid line), coefficients a (short dashed line), and b_ε (long dashed line) for chromium 3p **(a)** and neodymium 4d **(b)** excitations.

$$V_\varepsilon = \iint \psi_{\varepsilon d}(\mathbf{r}_1)\phi_{3d}(\mathbf{r}_2)\frac{e^2}{4\pi\varepsilon_0|\mathbf{r}_1 - \mathbf{r}_2|} \varphi_{3p}(\mathbf{r}_1)\varphi_{3p}(\mathbf{r}_2)d^3r_1 d^3r_2 \tag{16}$$

For excitations from inner shells that are more deeply bound, such as the 2p level (L_{23}) in the transitions elements or the 3d (M_{45}) level in the rare earths, this term becomes

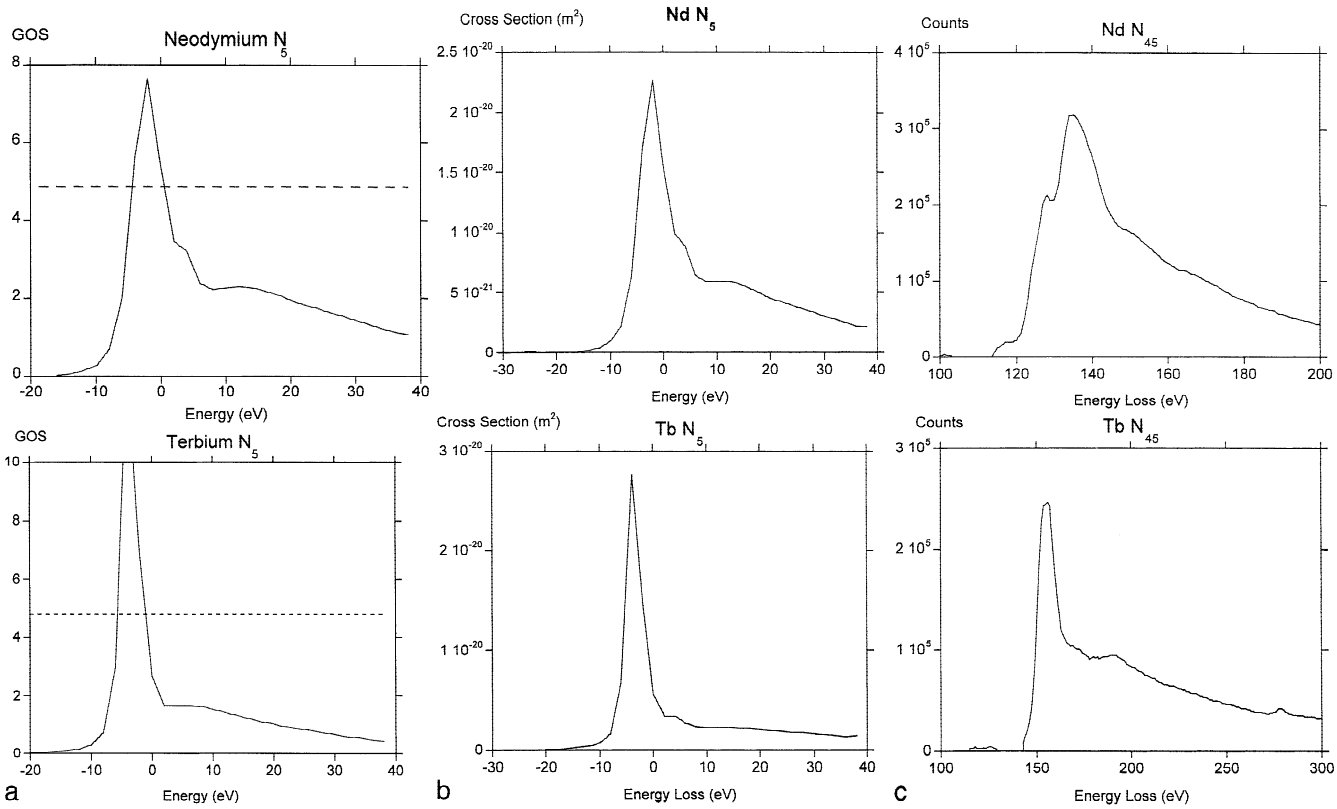

Figure 5. Generalized oscillator strength (GOS) (**a**); cross section for 100 kV electrons, 10 mrad collection angle (**b**); and electron energy loss spectrometry (EELS) atlas experiment (**c**) for neodymium and terbium 4d (N_5) excitations. The separation between the $4d_{3/2}$ (N_4) and the $4d_{5/2}$ (N_5) levels is sufficiently small to make it not worthwhile to perform calculations for both levels, though they are superimposed in the experiment.

quite small and the effect disappears. The coefficients a and b can be calculated in terms of the parameter η

$$\eta(\varepsilon) = \frac{\varepsilon - \varepsilon_{3d} - F(\varepsilon)}{\pi V_\varepsilon^2} \tag{17}$$

as

$$a = \frac{1}{\pi V_\varepsilon} \frac{1}{(1+\eta^2)^{1/2}} \tag{18a}$$

$$b_\varepsilon = \frac{\eta}{(1+\eta^2)^{1/2}} \tag{18b}$$

where $F(\varepsilon)$ is given by

$$F(\varepsilon) = P \int \frac{V_{\varepsilon'}^2}{\varepsilon - \varepsilon'} d\varepsilon' \tag{19}$$

where P denotes the principal part of the integral. The term $F(\varepsilon)$ is quite small and can be neglected in most cases. The variation of V_ε^2 and the coefficients a and b is given as Figure 4 for chromium 3p and neodymium 4d excitations. The configuration interaction integral remains fairly constant over the entire energy range while the coefficient a is strongly peaked at the bound state energy. An appropriate physical picture is to assume that above the threshold there is constructive interference between the bound state and the continuum state, giving an enhanced final state wavefunction, while below the threshold there is destructive interference giving a reduction in amplitude. The width of the threshold peak is influenced by the width of the curve for the parameter a, which is linked to the magnitude of the configuration interaction integral. Far above threshold, the effect of the bound state is minimal, since the coefficient a tends to zero and b tends to 1, and the result is identical to a calculation with only transitions to continuum states. These effects are all well demonstrated by the calculated

generalized oscillator strengths and scattering cross sections (200 kV, 10 mrad collection angle) for neodymium and terbium 4d excitations shown in Figure 5. For comparison, experimental spectra from the electron energy loss spectrometry (EELS) atlas (Ahn and Krivanek, 1983) are also shown, although a quantitative comparison cannot be made since the EELS atlas data is not on an absolute scale and the experimental conditions are somewhat different. It is still gratifying to see that the calculation reproduces the narrower threshold resonance in terbium.

Conclusions

All scattering relevant for electron microscopy and analysis is based on Coulomb interaction. This gives a general form and a scale for the cross sections that applies to both elastic and inelastic scattering. We show that, for elastic scattering relevant for HAADF microscopy, it is important to use either the thermal-diffuse or atomic scattering factor cross section rather than the simple Rutherford form. We have also reviewed inner shell ionization cross sections and shown how the Fano resonance can make a large difference to the threshold cross sections for first row transition element 3p (M_{23}) excitations or rare earth 4d (N_{45}) excitations.

Acknowledgment

The author dedicates this article to Prof. Archie Howie.

References

Ahn CC, Krivanek OL (1983) *EELS Atlas.* Pleasanton, CA: Gatan, Inc. and ASU

Allen LJ (1993) Electron energy loss spectroscopy in a crystalline environment. *Ultramicroscopy* 48:97–106

Amali A, Rez P (1997) Theory of lattice resolution in high angle annular dark field images. *Microsc Microanal* 3:28–46

Auerhammer J, Rez P, Hofer F (1989) A comparison of theoretical and experimental L and M cross sections. *Ultramicroscopy* 30:365–370

Davis LC, Feldkamp LA (1977) Interaction of many discrete states with many continua. *Phys Rev B* 15:2961–2969

Egerton RF (1986) *Electron Energy Loss Spectroscopy in the Electron Microscope.* New York: Plenum

Fano U (1961) Effects of configuration interaction on intensities and phase shifts. *Phys Rev* 124:1866–1878

Hirsch PB, Howie A, Whelan MJ, Nicholson RB, Pashley DW (1965) *Electron Microscopy of Thin Crystals.* London: Butterworths

Jesson DE, Pennycook SJ (1995) Incoherent imaging of crystals using thermally scattered electrons. *Proc R Soc London, Ser A* 449: 273–393

Leapman RD, Rez P, Mayers DF (1980) K, L and M shell generalized oscillator strengths and ionization cross sections. *J Chem Phys* 72:1232–1243

Pennycook SL, Boatner LA (1988) Chemically sensitive structure-imaging with a scanning transmission electron microscope. *Nature* 336:565–567

Rez P (1984) Electron ionization cross sections for K, L and M shells. *X-ray Spectrom* 13:55–59

Rez P, Bruley J, Brohan P, Payne M, Garvie LAJ (1995) Review of methods for calculating near edge structure. *Ultramicroscopy* 59: 159–167

Schiff LI (1968) *Quantum Mechanics.* New York: McGraw Hill

Scofield JH (1978) K- and L-shell ionization of atoms by relativistic electrons. *Phys Rev A* 18:963–970

Starace AF (1974) Effect of virtual 4d-shell excitations on rare earth spectra. *J Phys B* 7:14–25